Arch-piers systems subjected to vertical loads: a comprehensive review of rotational, sliding and mixed collapse modes

Danila Aita, Riccardo Barsotti & Stefano Bennati

Archive of Applied Mechanics

ISSN 0939-1533

Arch Appl Mech
DOI 10.1007/s00419-020-01766-4

Springer

Arch Appl Mech
https://doi.org/10.1007/s00419-020-01766-4

ORIGINAL

Danila Aita · **Riccardo Barsotti** · **Stefano Bennati**

Arch-piers systems subjected to vertical loads: a comprehensive review of rotational, sliding and mixed collapse modes

Received: 9 March 2020 / Accepted: 26 August 2020

Abstract This paper presents a study of the stability and collapse modes of a system made up of a masonry arch resting on two piers subject to its own weight. It examines both semicircular arches and three different types of pointed arches commonly found in architecture, namely low-pointed, equilateral, and lancet-pointed arches. The collapse modes characterizing each type of arch-piers systems are then compared by extending the results obtained by the authors in previous work on stand-alone masonry arches of different shapes. The mechanical behavior of these systems is examined via Durand-Claye's method in order to follow the evolution of the stability area and determine the collapse modes of these masonry structures. The method takes into account both the bounded bending capacity of the arch cross section and the limited friction along the joints. Furthermore, the system's safe domain is determined in terms of the limit conditions for arch thickness, pier height and friction coefficient. As expected, arch-piers systems of different shapes exhibit different behaviors at collapse in terms of minimum thickness and collapse modes.

Keywords Masonry arches · Pointed arches · Arch-piers systems · Collapse modes · Finite friction · Minimum thickness · Durand-Claye's method

1 Introduction

The dimensioning of systems composed of a masonry arch resting on two piers is a problem that has been tackled by several authors starting as far back as the sixteenth century. The main issue addressed in the past was determining the minimum thickness of the piers so as to guarantee the stability of the arch-piers system. Such determinations were made by adopting various geometric sizing criteria, which depended on the arch's intrados shape (Derand), the arch's intrados shape and thickness (Ruiz), and the arch's intrados shape and thickness together with the height of the overload and piers (Gil de Hontañón). Some scholars have offered detailed historical analyses of some of these rules, trying to contextualize them according to the building practices of the time. In this regard, without pretending to be exhaustive, we refer the interested reader to the treatise by Frézier [1] and historical analyses by Sanabria [2], Huerta [3,4], Benvenuto [5], Sacco [6], Becchi and Foce [7], and Sakarovitch [8]. It is interesting to note that the historical Spanish contributions offer a sort

D. Aita (✉) · R. Barsotti · S. Bennati
Department of Civil and Industrial Engineering, University of Pisa, Pisa, Italy
E-mail: danila.aita@unipi.it

R. Barsotti
E-mail: r.barsotti@ing.unipi.it

S. Bennati
E-mail: s.bennati@ing.unipi.it

Published online: 19 September 2020

of register of the proper dimensions for different structural elements, the Italian treatises, from Alberti [9] to Guarini [10], instead focused on proportional and geometrical rules according to aesthetical and geometrical criteria, whereas French scholars—starting with Philibert Delorme [11]—seemed to have a greater interest in stereotomy and sizing from a practical point of view, which later also involved mechanical aspects, as begun by Philippe De La Hire [12,13].

Finding the limit thickness in arch-piers systems so as to prevent collapse is an intriguing issue not only from a historical and architectural point of view, but also with regard to mechanical aspects. Buti and Corradi [14], Foce and Sinopoli [15], Sinopoli [16] and some contributions by the authors [17,18] offer mechanical interpretations of some historical sizing rules via equilibrium or kinematic analysis.

To the authors' knowledge, however, a systematic analysis is still lacking of the collapse modes occurring in arch-piers systems when the friction coefficient is finite. Given the significance of this issue, the present paper aims to illustrate some first results of and reflections on a parametric equilibrium analysis of these systems under the hypothesis of finite friction. Some limitations to the analysis must, however, be noted, namely we focus our attention solely on symmetric systems in which the arch and piers are subject to their own weight and have the same thickness, so as to determine the maximum pier height compatible with equilibrium and compare the mechanical response of arch-piers systems of different shapes, as well. The equilibrium analysis will be performed through a revisitation of an interesting historical method, i.e., Durand-Claye's method [19,20], which allows for taking into account the influence of both the friction coefficient and the compressive strength. This method has already been described by the authors in some previous works. For more detail, the interested reader is referred to [21–23].

In order to provide some background for the present contribution, it seems worthwhile recalling some works aimed at finding the minimum thickness of arches subjected to their own weight alone [24–27], conducted according to Milankovitch's geometric formulation of thrust line analysis [28,29]. In these studies, an infinite friction coefficient is assumed, so that sliding is ruled out by hypothesis. For the purposes of the present research, it is also worth citing a set of studies aimed at determining the minimum arch thickness under the hypothesis of a limited friction coefficient and infinite compressive strength [30–32].

A number of contributions within the current literature address the problem of arch-piers systems by also considering more complex load conditions than the ones presented in the present paper. In these works, horizontal and vertical loads, both in the static and dynamic regime, are considered and the corresponding problems are solved by means of numerical methods. In this regard, see, for example—without pretending to be complete—Zampieri et al. [33], who investigate the structural behavior of existing masonry bridges subject to local pier scour with a finite element model, or the work by Pulatsu et al. [34], in which DEM is utilized to evaluate the in-plane response of masonry arch-pier structures subject to horizontal static loads with steel tie reinforcement. With respect to these contributions, all based on numerical procedures, it should be pointed out that the purposes as well as the perspective adopted in the present research are different. Namely, a semianalytical approach, based on a revisitation of Durand-Claye's method, is reworked and applied to arch-piers systems of different shape, in order to perform a comprehensive parametric investigation on the collapse modes as the arch's thickness, friction coefficient and pier's height vary. This approach allows for explicitly identifying the limit conditions corresponding to the activation of symmetrical rotational, mixed (rotational + sliding), and sliding collapse modes.

This paper directly extends to arch-piers systems the results obtained by the authors in [22,23] for masonry arches of different shapes. The same four shapes considered in [23], *i.e.*, circular, low pointed, equilateral pointed, and lancet pointed, are analyzed here. Moreover, as will be shown in the following, the same analysis methods are exploited. The paper is organized as follows. Section 2 illustrates the methodology adopted in order to evaluate the stability of arch-piers systems, starting with a case study (a system composed of a low-pointed arch and piers). For this type of arch-piers system the safety domain in the parameters' space is obtained, and the corresponding collapse modes accurately described. Section 3 applies the procedure described in Sect. 2 to evaluate the stability of systems made up of circular and pointed arches and piers. The analysis is first conducted considering a high (or infinite) friction coefficient (Sect. 3.1), and then by examining the influence of the finite friction coefficient on the safe domain and collapse behavior of the systems. Furthermore, the collapse behavior of the different systems under examination is compared (Sect. 3.2). Finally, some concluding remarks (Sect. 4) highlight the complexity of this issue in the case of finite friction and present further developments of this research.

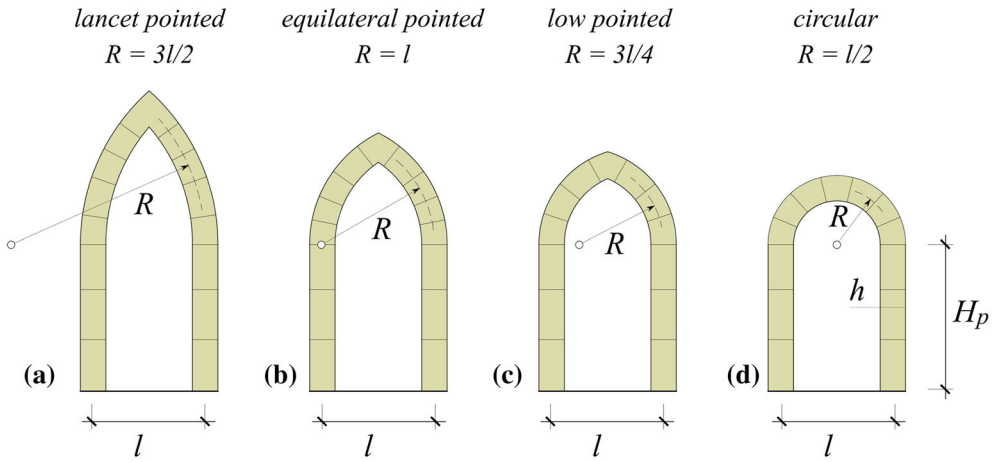

Fig. 1 The four arch-piers types considered

2 Limit analysis of arch-piers systems

Let us consider the masonry structural system formed by an arch connected to vertical piers (Fig. 1). Such a system is commonly found in the vertical walls of historical buildings and constructions, where it usually bears some vertical loads produced by the weight of the wall as well as that of the structures connected to the wall itself. In addition, horizontal static thrusts transmitted from adjacent domes and vaults, as well as horizontal seismic loads, may act on such arch-piers systems.

A complete analysis of the many different collapse conditions affecting an actual arch-piers system is all but simple to perform because of the many unknowns and uncertainties influencing the loading conditions as well as the complex structural interactions between the arch-piers system and surrounding elements. The analysis herein aims to provide a first comparison between the performance of differently shaped arch-piers systems in terms of load capacity. In particular, we consider the well-known simple benchmark problem, in which the arch-piers system is considered isolated from the rest of the masonry construction and the load consists solely of the system's own weight. Moreover, for the sake of simplicity, the same constant thickness and friction coefficient are assumed for both arch and piers. The masonry's strength is kept constant, and the system limit collapse conditions are analyzed by varying three main parameters, namely: the thickness, h, the piers' height, H_p, and the friction coefficient, μ, along the joints.

Note that the simplifying assumption adopted here—according to which both arch and piers have the same constant thickness—is a common choice in architecture and is even illustrated in historical treatises (see for example Leonardo da Vinci [35], Fig. 2). Despite its simplicity, this assumption allows for focusing on three significant parameters: arch thickness, pier height and friction coefficient, providing a comprehensive catalogue of all possible symmetric collapse modes occurring in arch-piers systems subjected to their self-weight. The fourth parameter, i.e., the ratio between arch and pier thicknesses, will be accounted for in the analysis in a further stage of the research. The reader interested in this topic is referred to [17,18], where some of the historical sizing rules related to the design of arch-piers systems are examined from a mechanical point of view. It is noteworthy that in these cases the limit condition also corresponds to one of the collapse modes included in the catalogue provided by the current parametric analysis, according to which an extrados hinge is formed at the pier's base. More details on this issue will be clarified in the following sections. For the purposes of the current paper, let it suffice to note that the method proposed here can be applied to symmetric arch-piers systems of any geometry.

With reference to Fig. 1, we consider lancet pointed (a), equilateral-pointed (b), low-pointed (c) and circular (d) arch-piers systems. For the sake of comparison, all the results shown in the following have been obtained assuming a compressive strength $|\sigma_c| = 20$ MPa, and nil tensile strength. Such values have been selected—from the many possible alternatives—to represent masonry of medium strength (e.g., sandstone masonry). Furthermore, the same span ($l = 10$ m), unit width (1 m) and specific weight ($\gamma = 20\,\text{kN/m}^3$) have been considered for each of the four arches. In passing, it should however be noted that very similar results would be obtained by assuming higher values, or even $|\sigma_c| = \infty$, for the compressive strength, since

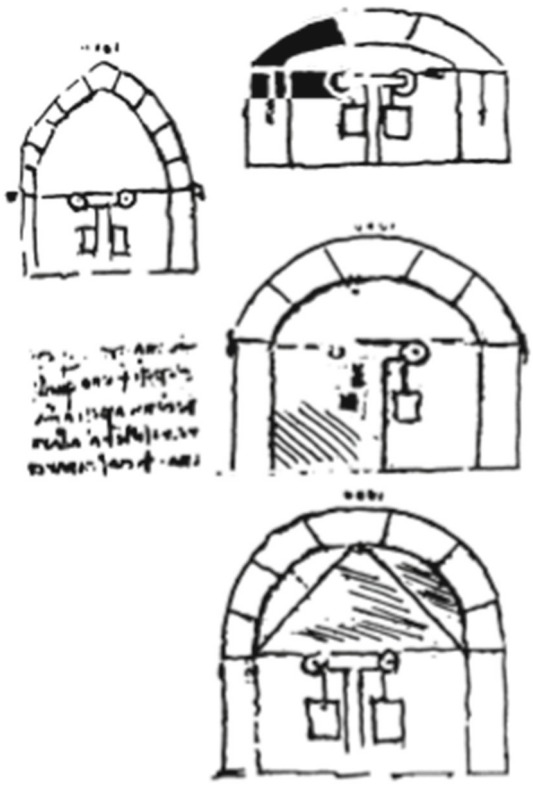

Fig. 2 Leonardo da Vinci, Forster Code II, fol. 82v

the masonry's compressive strength has only a weak influence on the mechanical behavior of arches subjected to their own weight alone.

The problem of determining the collapse condition for a given arch-piers system can be effectively dealt with using the Durand-Claye method, which is one of a number of graphical procedures developed in the 19th century to determine the line of thrust in arches. It aims to define the so-called area of stability at the crown section of a symmetric arch, that is to say, the locus of points formed by the extremes of the vectors representing admissible crown thrusts, i.e., those verifying the equilibrium of the structure and that are at the same time compatible with the masonry's strength [19,20]. A revised and enhanced version of this method, able to account for a nonlinear stress distribution in both tension and compression, has been introduced and described in some previous works by the authors [22,23]. In particular, [23] presents a detailed analysis of the collapse conditions affecting arches of different shapes subject to their own weight. The following illustrates an extension of the aforementioned procedure in order to consider the piers that bear the arch, as well.

2.1 Analysis of the collapse modes of arch-piers systems via a revised Durand-Claye's method

Let us consider the arch-piers system shown in Fig. 3a. The arch has a circular line of axis and radial cross sections of constant thickness h. The position of each cross section is given by the angle θ, with $\beta \leq \theta \leq \pi/2$. The piers are vertical, with horizontal cross sections of the same constant thickness h as the arch.

In our scheme, the masonry making up the arch and piers is viewed as an ideal homogeneous material, approximating in some mean sense the actual masonry. The limited bending and shear capabilities of actual masonry structures are accounted for, albeit only approximatively, by assuming that only compressive normal stresses may be transmitted across any cross section, at least up to a given threshold level. In other terms, we assume that ideal masonry has nil tensile strength, σ_t, and limited compressive strength, σ_c. Moreover, we also assume that a bounded shear force may be transmitted across any radial joints in the arch and horizontal joints in the piers.

As pointed out in [21,23], the original method proposed by Durand-Claye [19] assumes nil tensile strength, $\sigma_t = 0$, finite compressive strength, σ_c, and finite friction: any given cross section is subdivided into a non-

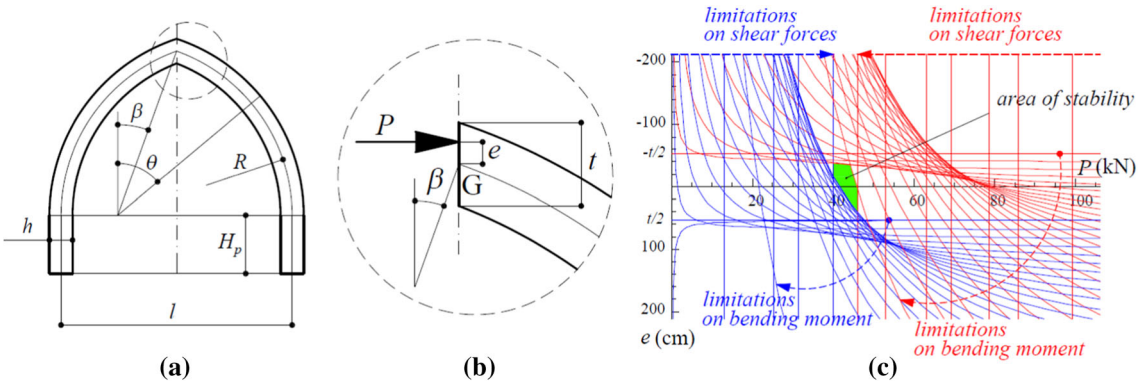

Fig. 3 The masonry arch-piers system(**a**); a detail of the crown section (**b**); an example of the area of stability according to Durand-Claye's method ($h = 1$ m, $R = 7.5$ m, $\mu = 0.25$, $H_p = 2.5$ m) (**c**)

reactive part where the normal stresses are zero, and a reactive part where the normal stresses vary linearly. In [20] Durand-Claye also considers finite tensile strength. The authors have modified the original version of the method, by assuming that the limit condition at each joint is reached when a bi-rectangular distribution of the stresses occurs. Such condition corresponds to the attainment of the limit value for the bending moment, which depends on the axial force as well as masonry's bounded compressive and tensile strengths, σ_c and σ_t [23] (application to the case in which $\sigma_t = 0$ is straightforward). Furthermore, as already provided for by the original formulation of the method, we assume that the shear force on any cross section is limited by friction, and a finite value for the friction coefficient, μ, is assumed. It is worth noting that Durand-Claye's approach allows for clearly distinguishing the influence of the friction coefficient from that of the shear strength on the arch's stability. In the current work, only the limitations related to friction have been taken into consideration, *i.e.*, there are no shear limitations for unlimited friction coefficient. Further details on this issue are examined in [21].

As illustrated in detail in a previous work by the authors [23], Durand-Claye's method allows for determining the complete set of all statically admissible distributions of internal forces, which can be effectively represented by the *area of stability*. By assuming that the joints under the arch's springing are horizontal, this procedure can be suitably adapted in order to consider the piers bearing the arch, as well.

Let us indicate with P and e the crown thrust and its eccentricity with respect to the cross-section's center of gravity, G, respectively (Fig. 3b). The assumed limitations on the masonry strength and friction coefficient enable determining the corresponding boundaries at the cross-sectional level of both the bending moment and shear capacities. By scanning all joints along the arch-pier system, a double set of limitations can be obtained and represented graphically in the (P, e) plane. The so-called *area of stability*, coloured green in Fig. 3c, is obtained by considering the region formed by the points of coordinates (P, e) that fulfil all the aforementioned limitations. When such an area shrinks to a point (or to a segment) the system attains a limit equilibrium condition, i.e., there is only one admissible value left for the crown thrust. From an operational point of view, a numerical procedure has been developed by means of an expressly formulated algorithm implemented in Mathematica®to account for the finite values of masonry tensile and compressive strengths, as well as the friction coefficient. The numerical procedure allows for plotting the curves corresponding to the attainment of the limit bending moment in the (P, e) plane. In Fig. 3c, red and blue curves correspond to positive and negative limit bending moment, respectively. The second set of limitations follows from the bounded shear capacity of the cross section, due to the limited friction coefficient, μ. In Fig. 3c, straight red lines correspond to the resultant of the internal forces tangential to the upper side of the friction cone (from a kinematic point of view, outwards sliding of the arch portion above the joint could occur), while straight blue lines correspond to the resultant of the internal forces tangential to the lower side of the friction cone (inwards sliding of the arch portion above the joint could occur). In the calculations, a finite number of radial joints are considered by subdividing the half arch's intrados into $n = 20$ equal parts. Although the numerical procedure allows for a greater number of subdivisions, the chosen value for n enables providing sufficiently accurate results as is illustrated in the following. More details on the numerical procedure are given in [21] and [23].

This method enables studying both the static and kinematic aspects of symmetric arch-piers systems. For further detail, the interested reader is referred to [23], where the collapse modes corresponding to different limit equilibrium conditions are determined for masonry arches. It is straightforward to conclude that the set of

Table 1 Equilibrium limit conditions corresponding to each collapse mechanism

	Symmetric collapse modes									
	Rotational		Sliding		Mixed (rotational + sliding)					
	1	2	5	6	3	4	9	8	7	10
1st joint	●	●	▬	▬	●	●	▬	●	●	▬
2nd joint	●	●	▬	▬	●	▬	●	●	▬	●
3rd joint	●	●			▬	●	●	▬	●	●

Symbols and notation adopted for the joints where a limit condition is attained

Limit equilibrium condition	**Kinematics**	**Symbol**
Positive limit bending moment	Relative rotation	●
Negative limit bending moment	Relative rotation	●
Limit shear force (upper side of the friction cone)	Relative sliding	▬
Limit shear force (lower side of the friction cone)	Relative sliding	▬

possible collapse modes for arch-piers systems coincide with that already determined for arches. The possible collapse modes are listed in Table 1, drawn from [23].

The sequence of joints where an equilibrium limit condition is attained has been ordered starting from the crown section (Table 1).

It should be noted that the results presented in the following sections focus on the stability of symmetric arch-piers systems. As the method also accounts for a limited friction coefficient along the joints, *non-standard* behavior is assumed for the arch-piers system: In the general case, neither the uniqueness of the collapse load, nor the validity of the static or kinematic theorems of limit analysis is assured. However, as pointed out in [23], for symmetric masonry arches the problem can be solved as if the material were *standard*. For this reason, the limit equilibrium conditions obtained via the Durand-Claye method enable determining the corresponding collapse mechanisms for a symmetric system when the analysis is limited to symmetric collapse modes. With no pretension to completeness, the interested reader is referred to [36–41] for some further remarks on *non-standard* behavior when finite friction is considered in both symmetric and non-symmetric equilibrium problems of arches and domes.

2.2 Application of Durand-Claye's method to the analysis of arch-piers system: the case study of low-pointed arch

2.2.1 The area of stability when no sliding is allowed

In order to illustrate the proposed analysis method in more detail, let us consider as a first example the low-pointed arch-piers system shown in Fig. 4a, which will be denoted in the following as LO1. We assume that the thickness h is large enough so that for $H_p = 0$ the arch alone would be stable ($h = 1$ m). In addition, we assume the friction coefficient is so high that no sliding is allowed between masonry units. If we increase H_p, starting from zero while h is kept constant, the system will attain a collapse condition when H_p reaches a threshold value, H_{Max}, whose value will depend on h. As shown in Fig. 4a, since in this first example no sliding is allowed, the collapse mechanism will be characterized by the rotational mode alone, more precisely, collapse mode #1 in Table 1. Figure 4a shows a plot of the corresponding thrust line, and the 'hinges' are denoted with red and blue points. This limit condition is defined by the vanishing of the stability area in Fig. 4b. The expressly developed numerical procedure allows for directly determining H_{Max} by imposing that the red curve corresponding to attainment of positive limit bending moment at the pier's base pass through the point of intersection between the two curves corresponding to limit bending moment at two joints, in this case identified by $\theta = 24°$ (red, positive bending moment) and $\theta = 69°$ (blue, negative bending moment).

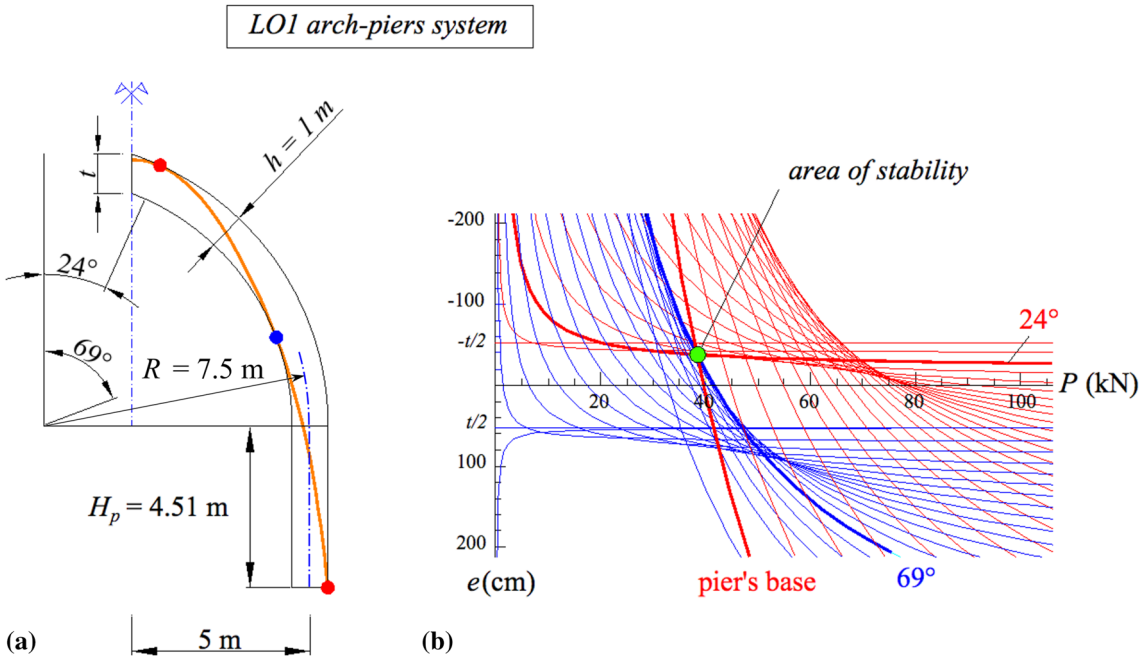

Fig. 4 The LO1 low-pointed arch-piers system in limit conditions when no sliding is allowed (**a**); the corresponding area of stability (**b**)

2.2.2 The area of stability when sliding is allowed

Let us consider a second example (Fig. 5a, LO2 arch), which refers to a low-pointed arch-piers system with the same thickness as before ($h = 1$ m). Contrary to the preceding example, here the friction coefficient is left free to take any value. Therefore, system collapse can take place through a larger set of possible mechanisms, potentially involving sliding or mixed rotational sliding modes when the friction coefficient becomes too low. If we again increase H_p, starting from zero while h is kept constant, and the friction coefficient μ is set equal to a 'sufficiently low' value (in the example, $\mu = 0.25$), the system will attain a collapse condition when H_p reaches a threshold value, H_μ, depending on both h and μ. As shown in Fig. 5a, since in this second example sliding is allowed, the collapse mechanism will be characterized by sliding, as well (collapse mode #10 in Table 1). It is straightforward to conclude that for a given h, $H_\mu \leq H_{\text{Max}}$.

In this case, the expressly developed numerical procedure allows for directly determining the value of H_μ by starting with the stability area (Fig. 5b). With reference to our case study, the limit condition is reached when the red curve corresponding to the attainment of the limit bending moment at the pier's base passes through the point of intersection between two curves: the straight blue line corresponding to a limit shear force at joint $\theta = 45°$, and the blue curve indicating the limit negative value for the bending moment at joint $\theta = 69°$.

2.2.3 A first parametric analysis: limit pier height and safe domain for low-pointed arch systems

Note that in order to perform a first parametric analysis of low pointed arches, the procedure described in paragraphs 2.2.1, 2.2.2 allows for determining the limit values of the height (H_{Max} or H_μ) by varying the arch thickness, h.

At first, let us assume an infinite friction coefficient, so as to prevent sliding. In this case, the piers' limit height, H_{lim}, corresponds to $H_{\text{Max}}(h)$. As observed above in Sect. 2.2.1, when $H_p = H_{\text{Max}}(h)$, the arch-piers system fails according to the rotational collapse mode #1, with one hinge located at the bottom of the piers (Fig. 4a).

Both the pier height and thickness can be put in dimensionless form by dividing them by the span l, i.e., by setting $\eta = H_p/l$ and $\zeta = h/l$. The limit curve $\eta_{\text{lim}} = \eta_{\text{Max}}(\zeta)$ is shown in Fig. 6a, where $\eta_{\text{Max}}(\zeta) = H_{\text{Max}}(h)/l$. As is evident from the figure, the values of $\eta_{\text{Max}}(\zeta)$ are increasing with ζ. The minimum value of η_{Max} is equal to zero and corresponds to the minimum value of ζ compatible with the system's equilibrium, which will be denoted as ζ_{min} (see the point LO in Fig. 6a corresponding to the stand-alone arch, $\zeta_{\text{min}} = 0.0405$).

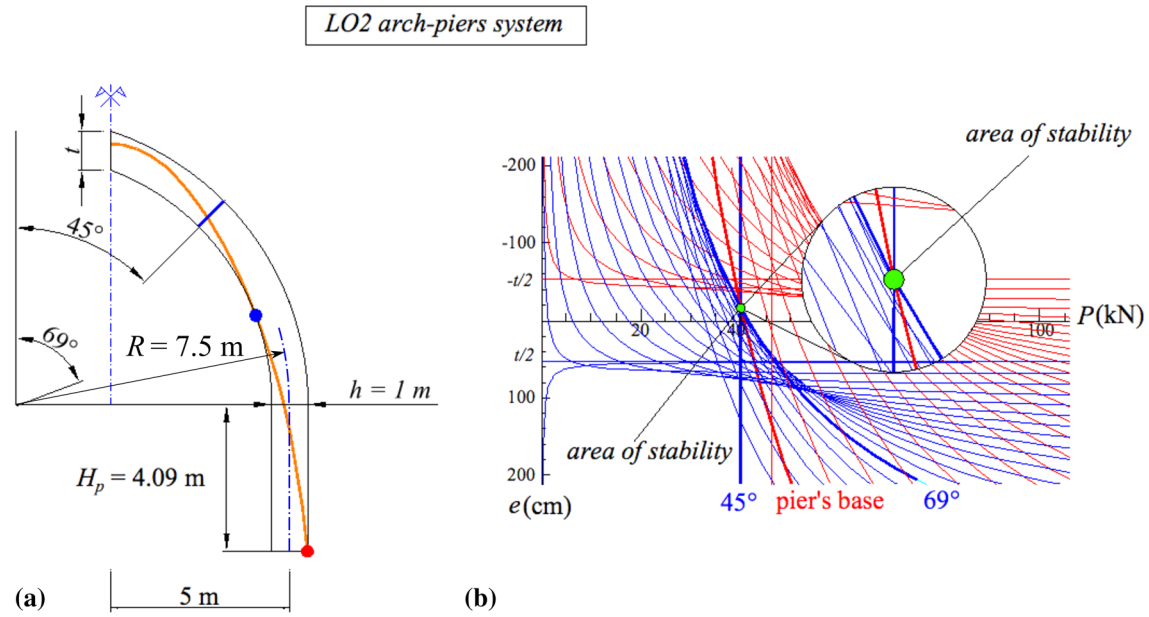

Fig. 5 The LO2 low-pointed arch-piers system in limit conditions when sliding is allowed (**a**); the corresponding area of stability (**b**)

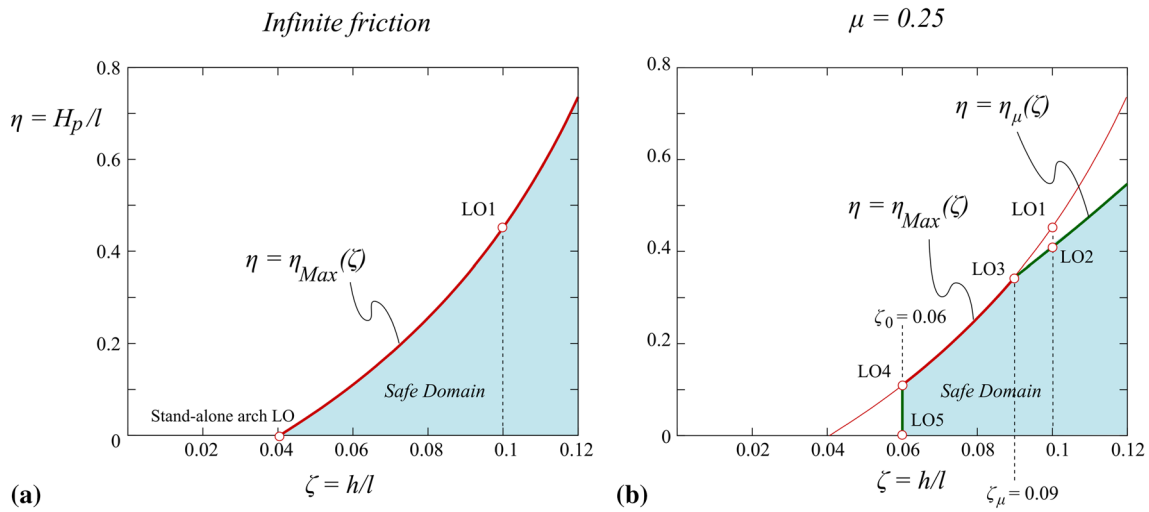

Fig. 6 Safe domain in the (ζ, η) plane for a low-pointed arch and piers system: **a** infinite friction; **b** finite friction ($\mu = 0.25$)

The region of the plane (ζ, η) under the limit curve $\eta_{\text{Max}}(\zeta)$, i.e. $\eta < \eta_{\text{Max}}$, coloured blue in Fig. 6a is the safe domain for the arch-piers system.

The points corresponding to the two examples illustrated in Sects. 2.2.1 and 2.2.2 are also shown in Fig. 6. In the (ζ, η) plane in Fig. 6a, point LO1 corresponds to the arch-piers system shown in Fig. 4a, whose thickness is equal to 1 m ($\zeta = 0.1$).

The point corresponding to the LO2 system is plotted in Fig. 6b, which shows the safe domain for a finite friction coefficient equal to $\mu = 0.25$.

As expected, slender systems collapse through rotational mode #1. On the contrary, when the thickness exceeds a threshold value depending on μ, sliding or mixed collapse modes take place. By way of example, by taking $\mu = 0.25$, the numerical procedure described above has allowed concluding that failure by sliding is prevented when the dimensionless thickness, ζ, is less than a limit value $\zeta_{\mu} = 0.09038$, which corresponds to the abscissa of point LO3 (Fig. 6b). In the case of $\zeta \leq \zeta_{\mu}$, the piers' limit height is determined by H_{Max}, and rotational collapse mode #1 occurs. Conversely, the given value of μ is not sufficient to prevent sliding when

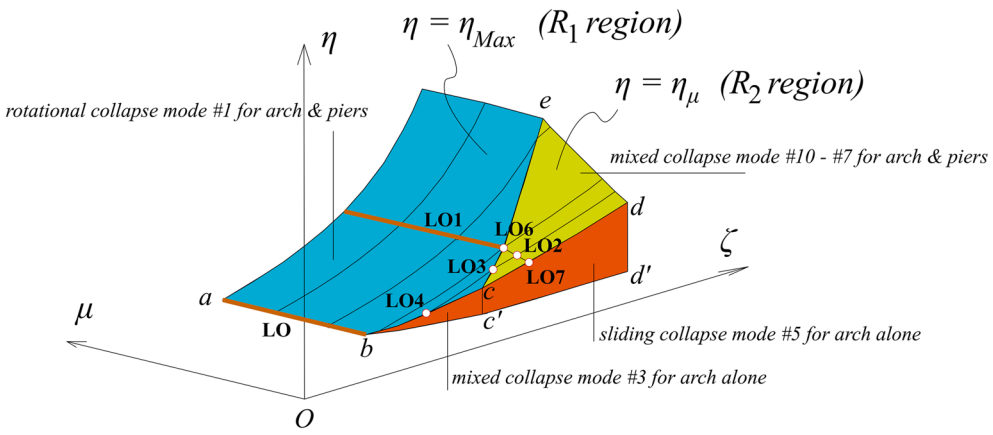

Fig. 7 3D safe domain for a low-pointed arch and piers system

$\zeta \geq \zeta_\mu$; in this case, the limit pier height corresponds to H_μ. When $\zeta = \zeta_\mu$, the relation $\eta_\mu = \eta_{\text{Max}}$ holds, and a transition between rotational collapse mode #1 and mixed collapse mode #10 occurs. Note that a limited friction coefficient also affects the minimum thickness needed to guarantee equilibrium. For the example under examination, i.e., for $\mu = 0.25$, equilibrium is possible for ζ larger than the minimum value $\zeta_0 = 0.06102$ (abscissa of point LO4, Fig. 6b). The condition identified by point LO4 corresponds to a transition between rotational collapse mode #1 (for the entire arch-piers system) and mixed collapse mode #3 (for the arch alone). Figure 8 shows the plots for the arch-piers systems considered in this example, which are examined in the following.

By fixing a value for the friction coefficient, $\mu = \bar{\mu}$, a limit curve $\eta_{\text{lim}}(\zeta, \mu = \bar{\mu})$, providing the limit pier height, H_{lim}, for each value of thickness, h, can be determined. The dimensionless admissible values of the pier height can be formally described by:

$$\begin{aligned} \eta &\leq \eta_{\text{Max}}(\zeta) \quad \text{if } \zeta_0 \leq \zeta \leq \zeta_\mu \\ \eta &\leq \eta_\mu(\zeta, \mu = \bar{\mu}) \quad \text{if } \zeta > \zeta_\mu \end{aligned}$$

2.2.4 Representation of the limit domain in the parameters' 3D space

The safe domain for the whole arch-piers system can be represented by determining, for each pair of (ζ, μ), the dimensionless limit pier height, η_{lim}. Through this procedure, which will be described in detail in the following, it is possible to determine the 3D safe domain in Fig. 7, where the significant points (LO1, LO2, LO3, LO4) represented in Fig. 6 have been reported. The blue surface represents the locus of points $(\varsigma, \mu, \eta_{\text{lim}})$ where $\eta_{\text{lim}} = \eta_{\text{Max}}(\zeta)$, and corresponds to an incipient rotational collapse mechanism (mode #1); the yellow surface is the locus of points $(\varsigma, \mu, \eta_{\text{lim}})$ where $\eta_{\text{lim}} = \eta_\mu(\varsigma, \mu)$, corresponding to an incipient mixed (rotational plus sliding) collapse mechanism (mode #10 or #7). The intersection between these two surfaces, represented by the curve (*c*-*e*), is the locus of points $(\varsigma, \mu, \eta_{\text{lim}})$ where $\eta_{\text{lim}} = \eta_{\text{Max}}(\varsigma) = \eta_\mu(\varsigma, \mu)$, and indicates a transitional collapse mode (#1-#10 or #1-#7) for the arch-piers system. The two orange surfaces correspond to collapse modes that do not affect the piers (mixed mode #3 and sliding mode #5 for the arch alone).

More in detail, the 3D domain in Fig. 7 can be obtained by starting with the results obtained by the authors in [23], i.e. by considering the set of (ζ, μ) pairs compatible with equilibrium of the arch alone. It is straightforward to conclude that the safe domain for the arch considered as a stand-alone structure will include the safe domain for systems with piers of any given height. For each pair (ζ, μ), the dimensionless pier height, η_{lim}, is then determined.

For the sake of clarity, Fig. 8 shows the projection of the safe domain of systems composed of a low-pointed arch and piers onto the coordinate plane (ζ, μ). The domain's projection can be subdivided into two regions: R_1 and R_2. Systems whose representative points fall into region R_1 collapse by rotation; on the contrary, in region R_2 system collapse is characterized by some sliding.

With reference to Fig. 8, we start by considering once again the low-pointed arch LO1 (see Fig. 4a). In the R_1 region of the (ζ, μ) plane, a whole half-line parallel to the μ axis corresponds to this system.

By maintaining the same dimensionless thickness ($\zeta = 0.1$) and decreasing the friction coefficient to $\mu = 0.272$, a transitional collapse mode #1-#10 occurs for the arch-piers system (point LO6 on the transition

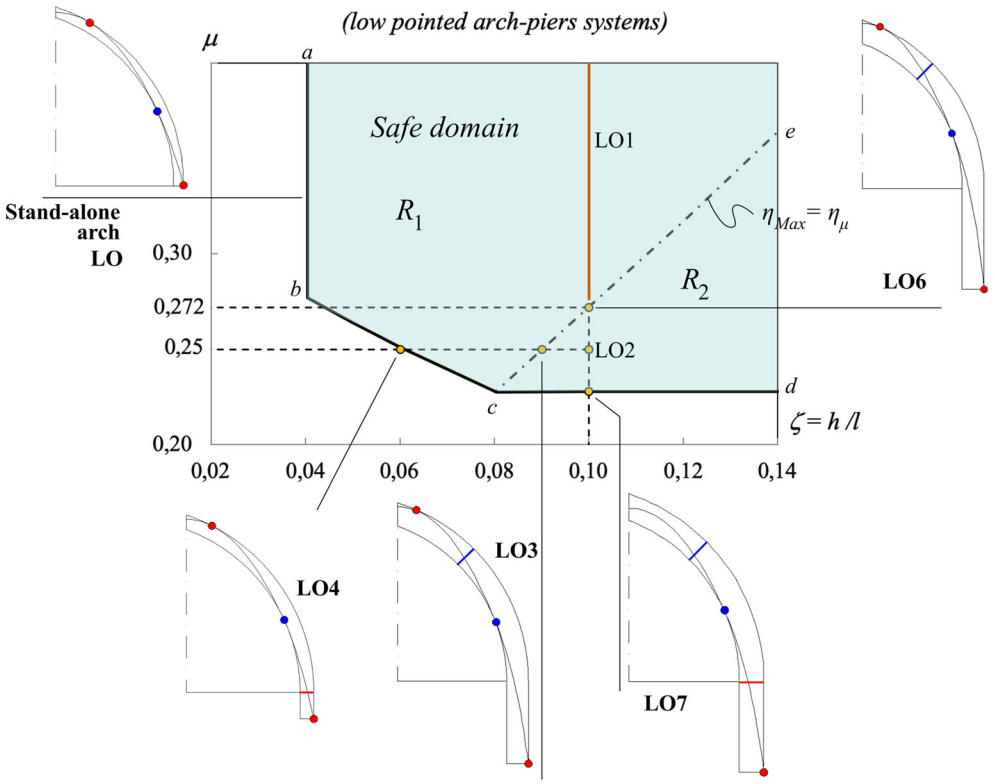

Fig. 8 Projection of the safe domain on the (ζ, μ) plane for a low-pointed arch and piers system

curve c-e). By further decreasing the friction coefficient to $\mu = 0.25$, the point corresponding to the LO2 system, belonging to the region R_2, is reached (Fig. 5a). When the dimensionless pier height equals its limit value, η_μ, the mixed (rotational plus sliding) collapse mode #10 occurs.

By further decreasing the friction coefficient, point LO7 is reached (see Figs. 7 and 8), corresponding to $\mu = 0.228$, i.e. the minimum friction coefficient compatible with an equilibrium condition for the given value of ζ. In this case, a transition between mixed collapse mode #10 (for the arch-piers system) and sliding mode #5 (for the arch alone) occurs.

It is worth noting that the boundary curves (b-c) and (c-d) of the safe domain projection in the (ζ, μ) plane in Fig. 8 correspond to a mixed (rotational + sliding) or sliding collapse mode for the arch alone. More precisely, they identify the minimum values of the friction coefficient compatible with equilibrium of the arch alone, depending on ζ. Curve (a-b) corresponds to the minimum value of the dimensionless thickness, $\zeta_{\min}$, compatible with equilibrium when only rotational collapse modes are possible, as described in Sect. 2.2.1. Note too that the curves represented in Fig. 6a, b are surface sections of the 3D safe domain (Fig. 8) with planes $\mu = \bar{\mu}$.

It seems worthwhile recalling in passing that the results presented here have been obtained via a numerical procedure, i.e., the algorithm expressly developed in Mathematica® based on Durand-Claye's method. In this section, as well as in the following, the results regard a range of ζ values, more precisely $\zeta_{\min} \leq \zeta \leq \zeta_1$, where $\zeta_{\min}$ is the minimum value of the dimensionless thickness compatible with system equilibrium, defined in Sect. 2.2.1, while ζ_1 has been suitably chosen in order to consider a class of arch-piers compatible with architectural requirements, without however pretending to conduct an exhaustive analysis (although $\zeta_1 = 0.3$ has been assumed for the applications, for graphical reasons, some of the graphs are limited to a more restricted range of ζ values).

3 A parametric analysis: the safe domain for pointed and circular arch-piers systems

In order to compare the mechanical behavior of arch-piers systems of different shapes, in this section, we present the results obtained by applying the procedure described in Sect. 2 to the four selected arch-piers

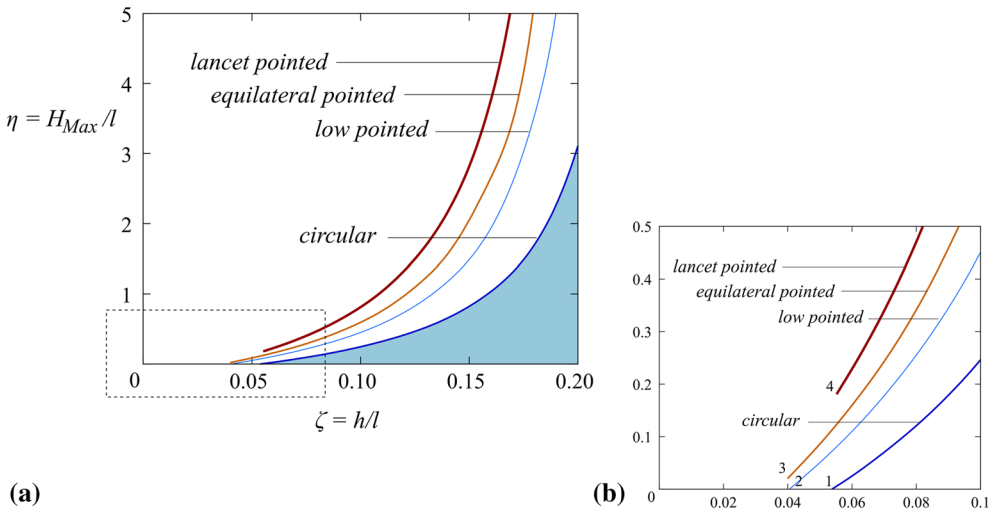

Fig. 9 Thickness-to-span ratio, ζ, versus limit pier height-to-span ratio, η_{Max}, when a high or infinite friction coefficient is assumed (**a**). Detail (**b**)

system types (Fig. 1), i.e. lancet, equilateral, low pointed, and circular. Recall that the parametric analysis is performed assuming the same span ($l = 10$ m), unit width (1 m) and specific weight ($\gamma = 20$ kN/m^3) for each of the four arches. For each of these systems, the safe domain is obtained, i.e., the limit dimensionless pier height, η_{lim}, is determined for each admissible point of the (ζ, μ) plane.

3.1 The safe domain for masonry arch-piers systems with infinite friction coefficient

As a first analysis, an infinite value of the friction coefficient is assumed. By proceeding as in the case study described in Sect. 2.2.1, for each value of the dimensionless thickness, $\zeta = h/l$, the limit dimensionless height of the piers, $\eta_{\text{Max}} = H_{\text{Max}}/l$, is determined. In all cases, the arch-piers system fails according to rotational collapse mode #1, with one hinge located at the pier base. The limit curve $\eta = \eta_{\text{Max}}(\zeta)$ for each arch type is plotted in Fig. 9a. By way of example, the safe domain is coloured blue for the circular arch.

The graph in Fig. 9a allows for making some comparisons between the collapse behavior of the four types of arch-piers systems. In this regard, it is worth noting that circular arches present the least extensive safe domain, whereas lancet pointed arches exhibit the most wide ranging. Equilateral pointed arches attain the absolute minimum value of the ratio h/l assuring stability ($h/l = 0.03993$). For all four arch-piers systems under examination, the values of $\eta_{\text{Max}}(\zeta)$ increase with ζ. For the minimum value of ζ compatible with equilibrium, ζ_{min}, the corresponding value of η_{Max} has been obtained.

Figure 9b shows a detail of Fig. 9a. As already observed in Sect. 2.2.1, when $\zeta = \zeta_{\text{min}}$, $\eta_{\text{Max}}(\zeta_{\text{min}})$ equals zero for low- pointed arch-piers systems. More precisely, $\eta_{\text{Max}}(\zeta_{\text{min}})$ also equals zero for systems made up of a circular arch with piers: collapse mode #1 occurs for the arch alone when $\zeta = \zeta_{\text{min}}$; this condition corresponds to points 1 (circular arches) and 2 (low pointed arches) in Fig. 9b and to the arch-piers systems in Fig. 10a, b. Equilateral and lancet pointed arches exhibit slightly different behavior, since the minimum value of ζ corresponds to activation of collapse mode #2 for the arch alone. In these cases, the corresponding value of η_{Max} is not equal to zero. Indeed, the arch alone would collapse according to collapse mode #2, i.e., without developing a hinge at the arch springing extrados. Therefore, the pier's limit height in these particular cases is conventionally determined as that corresponding to a hinge close to the extrados at the pier's base and to a transitional collapse mode #1-#2. In the (ζ, η) plane, this condition is represented by points 3 (equilateral pointed) and 4 (lancet pointed) in Fig. 9b. (The corresponding arch-piers systems are plotted in Fig. 10c, d).

3.2 The safe domain for masonry arch-piers systems with bounded friction coefficient

As noted in Sect. 2.2.2, characterizing the possible collapse conditions for an arch-piers system becomes more complicated when considering a finite value of the friction coefficient, μ. In such cases, depending on both

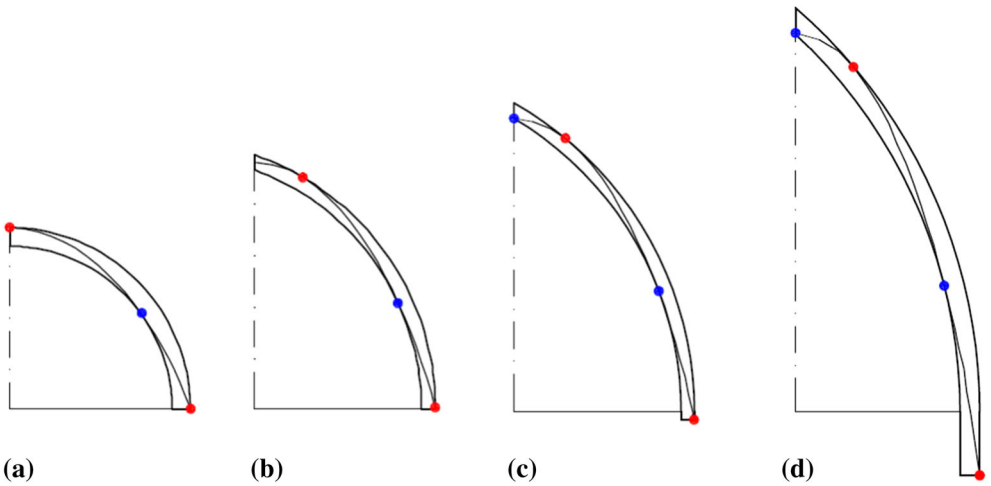

Fig. 10 Circular (**a**) and low-pointed arch (**b**) corresponding to points 1 and 2 in Fig. 9b; equilateral (**c**) and lancet pointed arch-piers system (**d**) corresponding to points 3 and 4 in Fig. 9b (transition between rotational collapse mode #2 for the arch alone and collapse mode #1 for the arch-piers system)

the dimensionless arch-pier thickness, ζ, and the friction coefficient, μ, system failure can occur according to either a rotational collapse mode (mode #1) or a rotational-sliding collapse mode (#10 or #7).

In order to compare the mechanical behavior of the four different arch-piers systems, Fig. 11 shows the limit curves corresponding to different values of the friction coefficient, namely $\mu = 0.25$, 0.35, 0.45, 0.55, 0.65, and 0.75. Note that the collapse condition depends heavily on the system's shape. For instance, a circular arch-piers system would collapse for $\mu = 0.25$, since this value is not admissible for the circular arch alone. On the other hand, equilateral and lancet pointed arches exhibit completely different behavior: With respect to the other types of arch-piers systems (circular and low pointed), considerably higher value for η_μ are obtained even for low values of the friction coefficient.

The results obtained in this section can be summarized in graphical form also by suitably adapting the safe domain diagrams for an arch plotted in the (ζ, μ) plane already described in Sect. 2 for the low-pointed arch-piers system. For further details on the safe domains of stand-alone arches of different shapes, the interested reader is referred to [23].

The results obtained for each of the four arch types are represented in Fig. 12, which provides the projection of the safe domain of the different arch-piers systems onto the coordinate plane (ζ, μ). In each diagram, the dashed line splits the domain in two. In the left-hand part, region R_1, the arch-piers system is stable provided that the piers' height is lower than the limit height, H_{Max}, at which point collapse mode #1 occurs. On the contrary, in the right-hand part of the safe domain, R_2, the arch-piers system is stable provided that the piers' height is lower than a limit value, H_μ (lower than H_{Max}). This second limit value, H_μ, depends on both the thickness, h, and friction coefficient, μ, and corresponds to activation of a mixed collapse mode for the arch-piers system (10 or 7). Lastly, if points (ζ, μ) belong to the dashed line, both collapse modes #1 and #10 (or #1 and #7) become possible if $\eta \geq \eta_{\text{Max}} \equiv \eta_\mu$.

The same remarks made for the low-pointed arch-piers systems with reference to Fig. 8 also apply to circular arch-piers systems, which exhibit analogous behavior—in terms of collapse modes—along curves (a), (b) and (c) (Fig. 12).

The results obtained for equilateral and lancet pointed arches (Fig. 12) reveal different behavior, in terms of collapse modes, along the domain's borders. Namely, with reference to Table 1, curve (a) corresponds to pure rotational collapse mode #2 for the arch alone and to transitional collapse mode #1–#2 for the arch-piers system, when $\eta \geq \eta_{Max}$ (see Fig. 10c, d). Curve (b) corresponds to collapse mode #9 for the arch alone, while additionally, if $\eta \geq \eta_{Max}$, rotational mode #1 becomes possible for the arch-piers system. Curves (c) and (d) correspond to sliding collapse modes #6 and #5 for the arch alone, and if $\eta \geq \eta_\mu$, the mixed collapse mode #10 (or #7) may also occur in the arch-piers system.

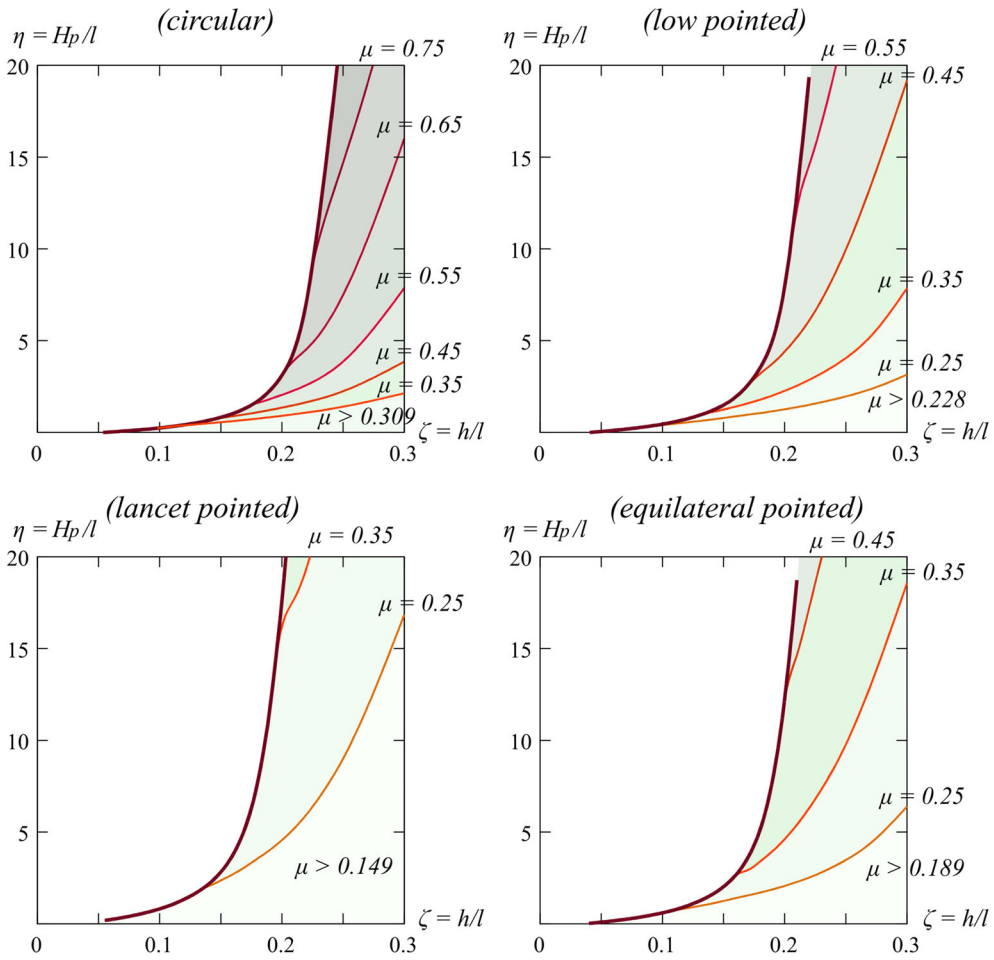

Fig. 11 Admissible domains for different values of friction coefficient μ for circular, low-pointed, equilateral, and lancet-pointed arches. $\zeta = h/l$ = thickness-to-span ratio; $\eta = H_p/l$ = pier height-to-span ratio

4 Concluding remarks

This paper presents a study of systems made up of an arch and the piers bearing it subjected to their own weight. Four classes of arch-piers systems are considered: circular, and low, equilateral and lancet pointed. The same span, unit width and specific weight are considered for each of the four types. Masonry is modelled assuming nil tensile strength and a high (or, in the limit case, infinite) value for compressive strength. Coulomb's law holds for frictional forces acting along the joints. Moreover, for the sake of simplicity, the arches and piers are assumed to have the same thickness.

The mechanical behavior of the four sets of arch-piers systems is examined via Durand-Claye's method in order to follow the evolution of the stability area and determine the collapse modes of each system. The safe domain is determined by defining the limit height of the piers compatible with the system's equilibrium and strength. More precisely, the influence of the friction coefficient on system collapse is thoroughly analyzed, and the dimensionless limit pier height values are obtained by varying both the dimensionless thickness and the friction coefficient. Moreover, a collapse mode is associated to each region of the safe domain by also examining the mechanisms corresponding to each segment of the safe domain border.

The results of the parametric analysis have shown that when the friction coefficient is considered infinite, the systems composed of a pointed lancet arch and piers present the most extensive safe domain: For each value of the arch's thickness, the values of the maximum pier height are greater than those attained by the other three system types. This result seems consistent with the choice of pointed arches in Gothic architecture, notably characterized, by slender buildings often of truly remarkable height. On the contrary, circular arch-piers systems correspond to the least extensive safe domain.

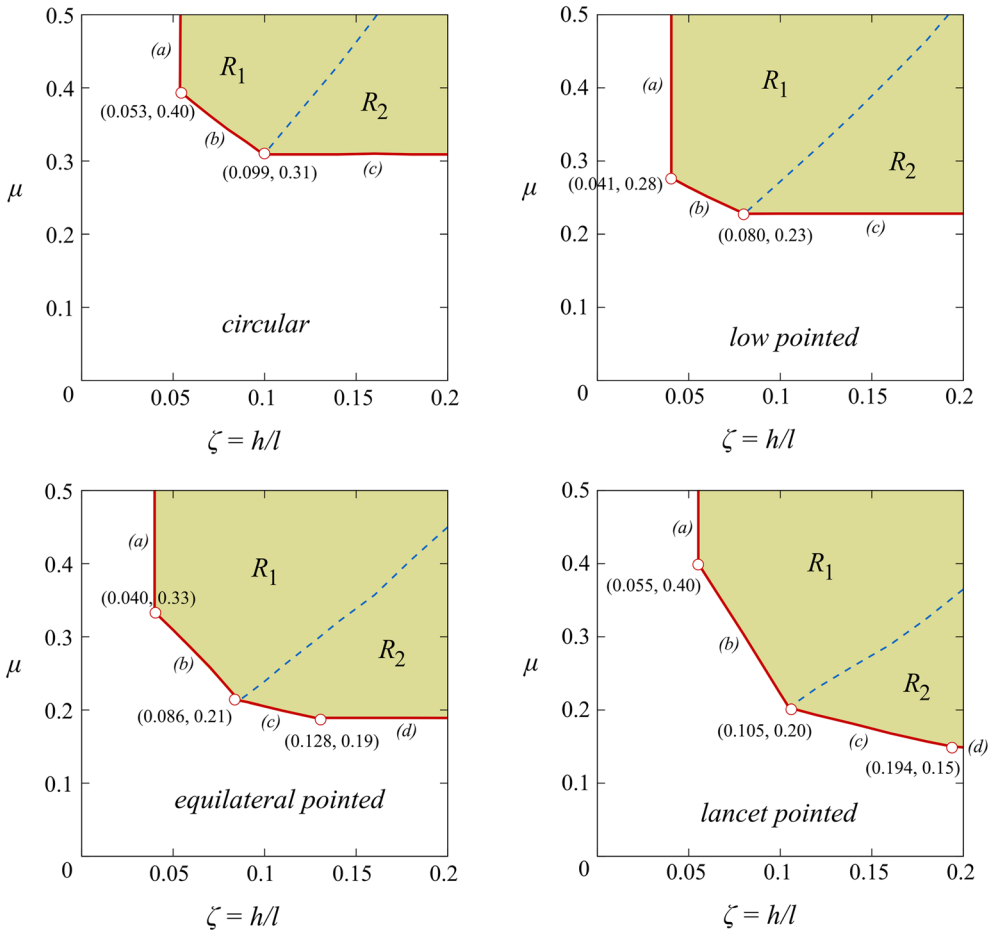

Fig. 12 Safe domain in the (ζ, μ) plane for arch-piers systems

The absolute minimum value of the ratio h/l assuring stability ($h/l = 0.03993$) is attained by systems composed of an equilateral pointed arch and piers, whereas the minimum coefficient compatible with equilibrium ($\mu = 0.149$) is attained by systems composed of a lancet pointed arch and piers. The minimum h/l ratio for circular or low-pointed arch-piers systems corresponds to the limit case in which the piers' height is zero (stand-alone arch); on the contrary, the pier's height is not equal to zero for equilateral or lancet pointed arch-piers systems.

When the friction coefficient is assumed to be finite, the equilibrium analysis shows that the arch-piers systems under examination collapse according to rotational collapse modes 1, 2, sliding collapse modes 5, 6, or mixed (sliding plus rotation) collapse mode 3, 7, 9, 10.

The method proposed allows for easily performing parametric investigations on the collapse of masonry arches by varying the main geometric and mechanical parameters involved and provides for accurate comparison—in terms of collapse behavior—between each of the systems under examination. Finally, this study clearly highlights the complexity of the collapse behavior of symmetrical arch-piers systems in the case of finite friction.

Compliance with ethical standards

Conflict of interest On behalf of all authors, the corresponding author states that there is no conflict of interest.

References

1. Frézier A.F.: La théorie et la pratique de la coupe des pierres et des bois pour la construction des voûtes et autres parties des bâtimens civils et militaires ou traité de stéréotomie à l'usage de l'architecture, 380–388, Strasburg-Paris (1737–1739)
2. Sanabria, S.L.: The mechanization of design in the 16th century: the structural formulae of Rodrigo Gil de Hontañón. J. Soc. Archit. Hist. **41**, 281–293 (1982)
3. Huerta, S.: Diseño estructural de arcos, bovedas y cupolas en España ca1500 - ca 1800. Tesis dirigida por Ricardo Aroca Hernandez Ros, Escuela Técnica Superior de Arquitectura de Madrid (1990)
4. Huerta Fernández, S.: The medieval 'scientia' of structures: the rules of Rodrigo Gil de Hontañón. In: Becchi, A., Corradi, M., Foce, F., Pedemonte, O. (eds.) Towards a History of Construction. Dedicated to Edoardo Benvenuto, series Between Mechanics and Architecture, pp. 567–585. Birkhäuser, Basel (2002)
5. Benvenuto, E.: La scienza delle costruzioni e il suo sviluppo storico. Sansoni, Firenze (1981)
6. Sacco, S.: "Coupe des pierres" e interpretazione statica del costruito nei trattati di stereotomia, tesi di laurea, Università di Genova (1997)
7. Becchi, A., Foce, F.: Degli archi e delle volte. Arte del costruire tra meccanica e stereotomia. Marsilio, Venezia (2002)
8. Sakarovitch, J.: Entre mécanique et géometrie: penser l'architecture clavée, l'exemple de Frézier. In: Becchi, A., Corradi, M., Foce, F., Pedemonte, O. (eds.) Towards a history of construction. Dedicated to Edoardo Benvenuto, series Between mechanics and architecture, pp. 587–600. Birkhäuser, Basel (2002)
9. Alberti, L.B.: De re aedificatoria. Nicolaus Laurentus, Florentiae (1485)
10. Guarini, G.: Modo di Misurare le fabbriche di d. Guarino Guarini C.R. teatino matem. di S.A.R. Eredi Giannelli, Torino (1674)
11. Delorme, Ph: Le premier tome de l'Architecture. F. Morel, Paris (1567)
12. La Hire, Ph. de: Traité de mécanique, où l'on explique tout ce qui est necessaire dans la pratique des Arts (1695), Mémoires de l'Académie Royale des Sciences, vol. 9, 1–333 (1730)
13. La Hire, Ph. de: Sur la construction des voûtes dans les édifices, Mémoires de l'Académie Royale des Sciences, année 1712, 69–77, Paris (1731)
14. Buti, A., Corradi, M.: I contributi di un matematico del XVII secolo ad un problema di architettura: Philippe de La Hire e la statica degli archi. Atti dell'Accademia ligure di scienze e lettere **38**, 303–323 (1981)
15. Foce, F., Sinopoli, A.: Per una teoria dell'analisi limite dell'arco murario come sistema di conci rigidi soggetti a vincoli unilaterali e attrito. In: De Pasquale, S. (ed.) Costruzioni voltate in muratura, Libreria Alfani Editrice. Firenze (2001)
16. Sinopoli, A.: A re-examination of some theories on vaulted structures: the role of geometry from Leonardo to De La Hire. In: Becchi, A., Corradi, M., Foce, F., Pedemonte, O. (eds.) Towards a History of Construction. Dedicated to Edoardo Benvenuto, series Between mechanics and architecture, pp. 601–624. Birkhäuser, Basel (2002)
17. Aita, D., Barsotti, R., Bennati, S.: Analysis of some historical sizing rules for arch-wall-piers systems. In: Biliszczuk, J., Bién, J., Hawryszków, P., Kamiński, T. (eds.), 8th International Conference on Arch Bridges. ARCH 2016. Arch Bridges in Culture, DWE, Wrocław, ISBN 978-83-7125-265-5 (extended abstract 426–429; paper on CD-ROM) (2016)
18. Aita, D., Barsotti, R., Bennati, S.: The collapse of a *magasin à poudre* described by Frézier: an interesting case study from the past. In: Ascione, L., Berardi, V., Feo, L., Fraternali, F., Tralli, A.M. (eds.) AIMETA 2017 - Proceedings of the XXIII Conference of the Italian Association of Theoretical and Applied Mechanics, pp. 1429–1437. Gechi Edizioni, Milano (2017)
19. Durand-Claye, A.: Note sur la vérification de la stabilité des voûtes en maçonnerie et sur l'emploi des courbes de pression. Ann. des Ponts et Chaussées **13**, 63–93 (1867)
20. Durand-Claye, A.: Note sur la verification de la stabilité des arcs métalliques et sur l'emploi des courbes de pression. Ann. des Ponts et Chaussées **15**, 109–144 (1868)
21. Foce, F., Aita, D.: The masonry arch between 'limit' and 'elastic' analysis. A critical re-examination of Durand-Claye's method. In: Huerta, S. (ed.) Proceedings of the First International Congress on Construction History, Madrid, 20–24 January 2003, vol. 2, pp. 895–908. Instituto Juan De Herrera, Madrid (2003)
22. Aita, D., Barsotti, R., Bennati, S.: Notes on limit and nonlinear elastic analyses of masonry arches. In: Aita, D., Pedemonte, O., Williams, K. (eds.) Masonry Structures: Between Mechanics and Architecture, pp. 237–264. Birkhäuser, Basel (2015). https://doi.org/10.1007/978-3-319-13003-3_9
23. Aita, D., Barsotti, R., Bennati, S.: Looking at the collapse modes of circular and pointed masonry arches through the lens of Durand-Claye's stability area method. Arch. Appl. Mech. **89**, 1537–1554 (2019). https://doi.org/10.1007/s00419-019-01526-z
24. Makris, N., Alexakis, H.: The effect of stereotomy on the shape of the thrust-line and the minimum thickness of semicircular masonry arches. Arch. Appl. Mech. **83**, 1511–1533 (2013)
25. Alexakis, H., Makris, N.: Minimum thickness of elliptical masonry arches. Acta Mech. **224**, 2977–2991 (2013)
26. Alexakis, H., Makris, N.: Limit equilibrium analysis of masonry arches. Arch. Appl. Mech. **85**, 1363–1381 (2015)
27. Nikolic, D.: Thrust line analysis and the minimum thickness of pointed masonry arches. Acta Mech. **228**, 2219–2236 (2017)
28. Milankovitch, M.: Beitrag zur Theorie der Druckkurven. Dissertation zur Erlangung der Doktorwürde, K.K. technische Hochschule, Vienna (1904)
29. Milankovitch, M.: Theorie der Druckkurven. Z. Math. und Phys. **55**, 1–27 (1907)
30. Sinopoli, A., Corradi, M., Foce, F.: Modern formulation for preelastic theories on masonry arches. J. Eng. Mech. **123**, 204–213 (1997)
31. Gilbert, M., Casapulla, C., Ahmed, A.H.: Limit analysis of masonry block structures with non-associative frictional joints using linear programming. Comput. Struct. **84**, 873–887 (2006)
32. Rizzi, E., Colasante, G., Frigerio, A., Cocchetti, G.: On the mixed collapse mechanism of semi-circular masonry arches, Structural Analysis of Historical Constructions – Jerzy Jasieńko (ed.), DWE (2012)
33. Zampieri, P., Zanini, M.A., Faleschini, F., Hofer, L., Pellegrino, C.: Failure analysis of masonry arch bridges subject to local pier scour. Eng. Fail. Anal. **79**, 371–384 (2017)

34. Pulatsu, B., Erdogmus, E., Bretas, E.M. Lourenço, P.B.: In-Plane Static Response of Dry-Joint Masonry Arch-Pier Structures, Architectural Engineering Institute (AEI) Conference, April 3–6 (2019)
35. Leonardo da Vinci, Forster Code II, fol. 82v, drawn from Benvenuto E., *An introduction to the history of structural mechanics*, Vol. II. Springer, New York (1991)
36. Boothby, T.: Stability of Masonry Piers and arches including sliding. J. Eng. Mech. **120**(2), 304–319 (1994)
37. Baggio, C., Trovalusci, P.: Collapse behaviour of three-dimensional brick-block systems using non-linear programming. Struct. Eng. Mech. **10**(2), 181–195 (2000)
38. Casapulla, C.: Dry rigid block masonry: safe solutions in presence of Coulomb friction. Trans. Built Environ. **55**, 251–261 (2001)
39. Simon, József, Bagi, Katalin: Discrete element analysis of the minimum thickness of oval Masonry Domes. Int. J. Archit. Herit. **10**(4), 457–475 (2016). https://doi.org/10.1080/15583058.2014.996921
40. Beatini, V., Royer-Carfagni, G., Tasora, A.: Modeling the shear failure of segmental arches. Int. J. Solids Struct. **158**, 21–39 (2019). https://doi.org/10.1016/j.ijsolstr.2018.08.023
41. Aita, D., Sinopoli, A.: Revisiting Monasterio's unpublished manuscript: a critical review of the collapse modes analysis of non-symmetric and symmetric masonry arches. Int. J. Archit. Herit. **14**(5), 762–793 (2020). https://doi.org/10.1080/15583058.2019.1648586